Preprints (www.preprints.org) | NOT PEER-REVIEWED | Posted: 15 August 2018 doi:10.20944/preprints201808.0276.v1

-reviewed version available at *Impact of Major Typhoons in 2016 on Sea Surface Features in the Northwestern Pacific* **2018**, *10*, 1326; doi:10.3390/w1010

Article

Impact of Major Typhoons on Sea Surface Environment in the Northwestern Pacific Derived from Satellite Remote Sensing

Dan Song [1], Linghui Guo [1,*], Zhigang Duan [2] and Lulu Xiang [1]

[1] Institute of Physical Oceanography and Remote Sensing, Ocean College, Zhejiang University, No. 1 Zheda Road, Zhoushan 316021, China; dsong@zju.edu.cn (D. Song); vivian_366@163.com (L. Xiang)
[2] 32020 Unit, Chinese People's Liberation Army, No. 15 Donghudong Road, Wuhan 430074, China; xikunlun2010@163.com (Z. Duan)
* Correspondence: linghguo@163.com (L. Guo)

Abstract: Studying the interaction between the upper ocean and the typhoons is crucial to improve our understanding of heat and momentum exchange between the ocean and the atmosphere. In recent years, the upper ocean responses to typhoons have received considerable attention. The sea surface cooling (SSC) process has been repeatedly discussed. In the present work, case studies were examined on five strong and super typhoons that occurred in 2016—LionRock, 1610; Meranti, 1614; Malakas, 1616; Megi, 1617; and Chaba 1618—to search for more evidence and new features of typhoon's impact on the sea surface environment. The typhoon monitoring data from the Central Meteorological Observatory, the sea surface temperature (SST) data from satellite microwave and infrared remote sensing, and the sea surface height anomaly (SSHA) data from satellite altimeters were used to analyze in detail: the SSC features caused by typhoons, the relationship between the SSC and the typhoon travelling speed, and the variations in cold and warm eddies during typhoon passage. Results showed that: (1) SSC generally occurred during typhoon passage and the degree of SSC was always determined by the strength and the travelling speed of the typhoon, as well as the initial SST. (2) One day before or on the day of typhoon passage, the SSHA slightly increased due to low surface pressure. After the typhoon passed, the SSHA obviously decreased along with the SSC. The pre-existing positive SSHAs, which always represent warm eddies, decreased or disappeared during typhoon passage, whereas negative SSHAs or cold eddies were enhanced. (3) New cold eddies were generated, especially at the turning points of the typhoon path. The presence of warm eddies is suggested to have a strengthening effect on the typhoons.

Keywords: typhoon; sea surface temperature; sea surface height anomaly; sea surface cooling; warm eddy; cold eddy

1. Introduction

The Northwestern Pacific Ocean is the largest ocean area with typhoons, hurricanes, or tropical cyclones, accounting for more than 30% of the total number worldwide [1]. As severe weather phenomena, typhoons not only cause serious damage to coastal areas, but also constantly change the marine hydrological environment during their passage. It is generally thought that typhoons play an important role in regulating the momentum, heat, and material exchange between the upper ocean and the atmosphere. Improving our understanding of typhoon-ocean interactions is required to formulate more accurate typhoon predictions [2–5].

During typhoon passage, the most obvious response of the ocean is the significant reduction in sea surface temperature (SST) [6], named sea surface cooling (SSC). The observed drop in SST could vary tremendously from about 2 °C [7] to even 11 °C [8]. The maximum cooling caused by a typhoon is mainly concentrated within 100 km to both sides of the typhoon path [9]. As a result of the wind

© 2018 by the author(s). Distributed under a Creative Commons CC BY license.

Preprints (www.preprints.org) | NOT PEER-REVIEWED | Posted: 15 August 2018 doi:10.20944/preprints201808.0276.v1

-reviewed version available at Impact of Major Typhoons in 2016 on Sea Surface Features in the Northwestern Pacific 2018, 10, 1326; doi:10.3390/w1010

entrainment, SSC caused by typhoons always appears to the right side of the track [10–12]. However, left side of the typhoon track may also experience higher SSC due to higher rainfall [13,14]. Typhoon-generated SSC and current velocity increases are often strongly rightward-biased, and shifts toward the typhoon track at depths exceeding roughly 100 m [15–17]. Additionally, the distance between the cooling center and the typhoon track depend mainly on the typhoon's travelling speed [18]. Moreover, studies have suggested that the degree of typhoon-induced SSC depends not only on the intensity of the typhoon and its travelling speed, but also on the mixing layer depth [8,9] and the pre-existing eddies [19–25]. By analyzing four typical tropical cyclones in the South China Sea, Zhang et al. concluded that the stronger the intensity of a tropical cyclones, the slower the movement speed, the shallower the mixed layer depth, and the greater the reduction in SST [24]. On the other hand, pre-existing cold eddies would enhance the SSC caused by the typhoons [8,26,27], whereas the SST drop in a warm-eddy-controlled region might not be very obvious [24,25].

Typhoons could also have a direct impact on the sea surface height field by pumping upwelling and enhancing vertical mixing, thus affecting the distribution of warm and cold eddies [19,23,28,29]. When a typhoon passes over, the sea surface height anomaly (SSHA) shows a drop and the mesoscale cold eddies are strengthened [21]. Yang et al. [21] revealed that the maximum cooling center of the SST caused by typhoons (three consecutive ones: Sinlaku 0813, Hagupit 0814, and Jangmi 0815) coincided with the regional center of the negative SSHA or mesoscale cold eddy, and the typhoons enhanced the pre-existing cold eddy. Liu [19], through the analysis of three typhoons (Lingling 0123, Chanthu 0405, and Durian 0621), found that the cold eddy on the right side of the typhoon's path strengthened, whereas the warm eddy on the path weakened after the typhoon passes.

In the present work, we examined case studies on the impact of five major typhoons that occurred in 2016 and passed through the Northwestern Pacific Ocean using remote sensing data analysis and focused on the following aspects: (1) impact of typhoon passage on SST and the relationship between the SSC and the pre-existing eddies; and (2) distribution of cold and warm eddies before and after the typhoon passage and the relationship between the eddies and the typhoon intensity. More evidence for SSC caused by typhoons was found and it was suggested that the previous existence of a warm eddy may enhance the typhoon during its passage.

2. Data and Methods

Five strong and super typhoons (Table 1) that occurred in the Northwestern Pacific Ocean from August 20, 2016 to October 5, 2016 were selected for case studies in the present work, including LionRock (1610), Meranti (1614), Malakas (1616), Megi (1617), and Chaba (1618). These five typhoons occurred consecutively with considerable impact, and followed three different types of path (Figure 1). The typhoon monitoring data were released by the Central Meteorological Observatory on the internet in real time (http://typhoon.nmc.cn/web.html). The data included typhoon center positions, minimum air pressures, maximum wind speeds, and average travelling speeds.

Table 1. Information about the five typhoons in 2016.

Name	Duration (h)	Path Type	Maximum Wind Speed (m/s)
LionRock 1610	276	Southwest to Northeast	50
Meranti 1614	147	Northwest (sea path)	70
Malakas 1616	177	Northwest to Northeast	52
Megi 1617	135	Northwest	52
Chaba 1618	180	Northwest to Northeast	60

Preprints (www.preprints.org) | NOT PEER-REVIEWED | Posted: 15 August 2018 doi:10.20944/preprints201808.0276.v1

-reviewed version available at Impact of Major Typhoons in 2016 on Sea Surface Features in the Northwestern Pacific 2018, 10, 1326; doi:10.3390/w1010

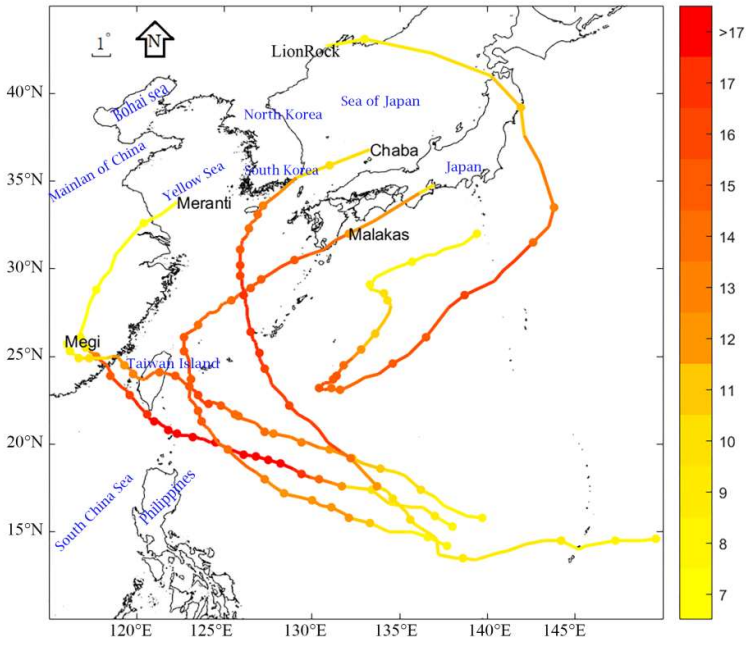

Figure 1. Paths map of five major typhoons in 2016. The dotted colored lines show the trajectories of the typhoons, and the color through each dot represents the intensity of the typhoon in levels of the Beaufort Wind Scale.

The SST data were obtained using microwave (MW) remote sensing (TMI, AMSR-E, AMSR2, and WindSat) and infrared (IR) remote sensing (Terra MODIS and Aqua MODIS). The time resolution is 1 day, and the spatial resolution is 9 km (ftp://ftp.remss.com/sst/daily_v04.0/mw_ir/). To avoid statistically insignificant effects, we considered the cooling of the typhoon track area during the typhoon's birth and disappearance as being caused by the typhoon crossing. Therefore, we selected the lowest temperature of the grid during the statistical period as the temperature after typhoon transit, and the temperature field of the previous day was subtracted from the temperature field generated by the typhoon to obtain the cooling distribution of the study area.

Satellite altimeters provided us with a useful method of obtaining long-term data on global sea surface height anomaly (SSHA), which has been proven to be in good agreement with in-situ observations, such as the tide gauge [30]. The SSHA data are released by the Satellite Oceanographic Data Center (AVISO) of the Centre National d'Etudes Spatiales through its official website. This data are mainly composed of TOPEX/POSEIDON, Jason-1, and ERS/Envisat altimeter satellites, with a time resolution of 1 day and a spatial resolution of 0.25°. The data included SSHA and geostrophic flow velocity (u/v) data. In the study area, the determination of the center and extent of cold and warm eddies was performed using the geostrophic velocity field.

3. Results

3.1. LionRock

Typhoon LionRock developed from a disturbance in the Pacific open ocean. It slowly moved northwestward under the guidance of the subtropical high, and the typhoon intensity gradually strengthened. On August 17-18, 2016, it encountered a high-level eddy in the troposphere, resulting in a significant reduction in convection and intensity. However, on August 19-20, it experienced the Fujiwhara effect (two typhoon inter-rotational effects) with the Kompasu in the development stage. It turned south and entered the relatively warm ocean surface. Convection occurred, and its intensity increased. LionRock developed into a tropical storm. Subsequently, on August 21-22, LionRock displayed the Fujiwhara effect with Typhoon Mindulle and continued to move

Preprints (www.preprints.org) | NOT PEER-REVIEWED | Posted: 15 August 2018 doi:10.20944/preprints201808.0276.v1

-reviewed version available at *Impact of Major Typhoons in 2016 on Sea Surface Features in the Northwestern Pacific* **2018**, *10*, 1326; doi:10.3390/w1010

southward. The Fujiwhara effect occurs when cyclones are in proximity to one another; their centers will begin orbiting cyclonically about a point between the two systems due to their cyclonic wind circulations [31].. It became a strong tropical storm and developed into a typhoon at 8:00 a.m. on August 24, with a maximum wind speed of 35 m/s. At 2:00 p.m., it developed into a strong typhoon with a maximum wind speed of 42 m/s and was oriented in the southwest direction. At 2:00 a.m. on August 26, LionRock was affected by the Western North Pacific subtropical high (WNPSH) and changed its direction from southwest to northeast, with its intensity gradually strengthening. At 2:00 p.m. on August 28, it developed into a super typhoon and maintained its strength until August 29 at 2:00 p.m. From 8:00 p.m. on August 29 to 2:00 a.m. on August 30, it gradually turned to the northwest. It made landfall in Japan at 5:00 p.m. on August 30 and reached Northeast China at 5:00 a.m. on August 31, 2016.

LionRock caused a certain degree of cooling (>2 °C) in a large area of the sea path (Figure 2). The cooling of the right side of the path was more obvious than that of the left side, and the cooling was greatest at the turning point of the typhoon path and when the typhoon wind speed was greater than 5 K. The cooling area at the turning point of the typhoon path was concentrated in a circular area. The cooling center of the typhoon straight-through area was about 100 km on the right side of the typhoon path, and the cooling area was also approximately circular with a cooling radius of about 200 km. The cooling in the Yellow Sea and the Sea of Japan in China was probably due to the effect of the Kuroshio. The SSHA distribution (Figure 3a) before the passage of Typhoon LionRockk was obviously related to the cooling distribution. From Figure 3a, before the typhoon crossing (August 19, 2016), where the SSHA value was positive (i.e., it was in a warm eddy area), the cooling was low (<3 °C). When the SSHA before a typhoon crossing is negative (i.e., it is in a cold eddy area), the cooling caused by LionRock was relatively high and the cooling eddy center was close to the center of the cold eddy. The SSHA distribution (Figure 3a) before the passage of Typhoon LionRock was obviously related to the cooling distribution. Before the typhoon crossing, where the SSHA value was positive (i.e., it was in a warm eddy area), the cooling was low (<3 °C). When the SSHA before a typhoon crossing was negative (i.e., it is in a cold eddy area), the cooling was relatively high and the cooling eddy center was close to the center of the cold eddy.

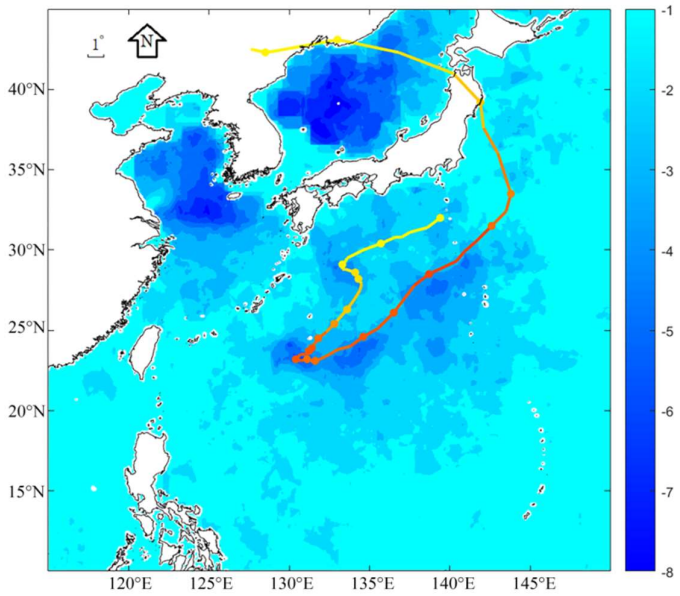

Figure 2. Cooling of the sea surface after Typhoon LionRock passed through. The color bar represents the degree of cooling in °C. The meaning of the color of the typhoon trajectory is consistent with Figure 1.

Preprints (www.preprints.org) | NOT PEER-REVIEWED | Posted: 15 August 2018 doi:10.20944/preprints201808.0276.v1

-reviewed version available at *Impact of Major Typhoons in 2016 on Sea Surface Features in the Northwestern Pacific* **2018**, *10*, 1326; doi:10.3390/w1010

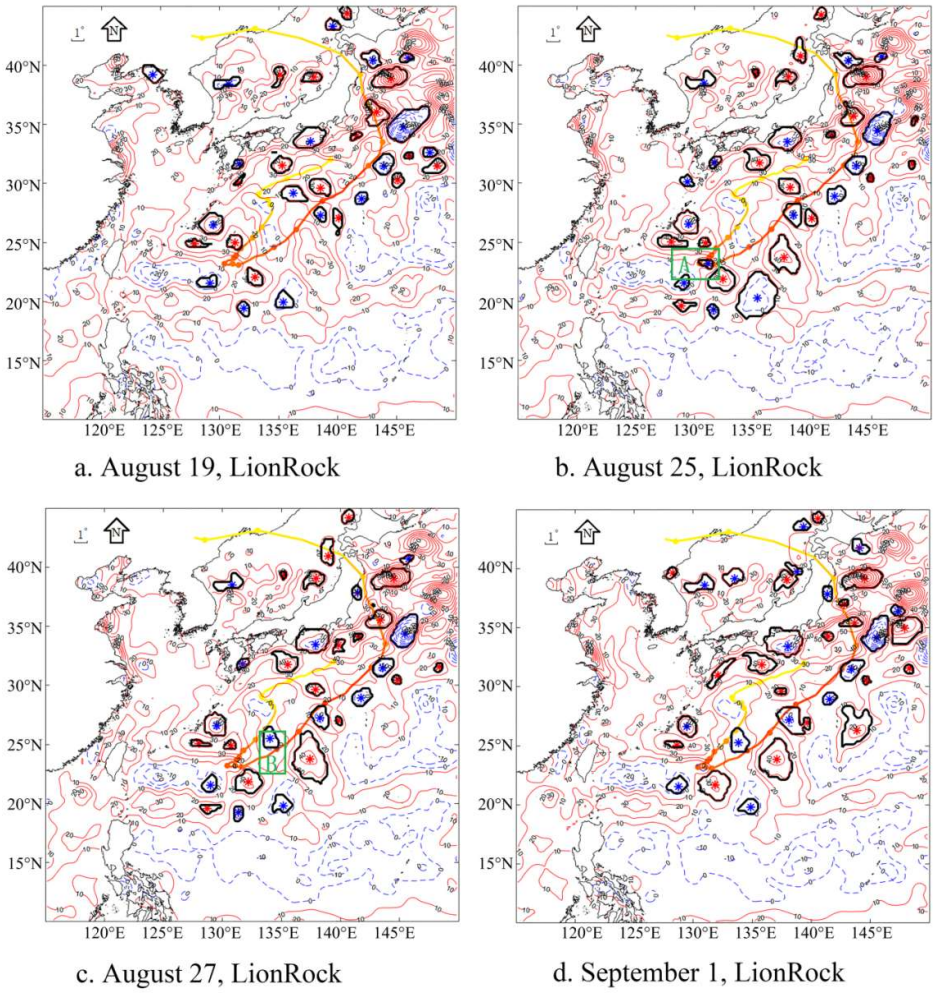

Figure 3. Distribution of cold and warm eddies alongside the path of Typhoon LionRock (**a**) before the typhoon was generated (August 19, 2016, (**b**) during the typhoon (August 25, 2016), (**c**) during the typhoon (August 27, 2016), and (**d**) after Typhoon LionRock passed (September 1, 2016). The color on the typhoon path is consistent with Figure 1. The bold black solid line outside the blue * (cold eddy) and the red * (warm eddy) represents the boundary of that eddy. Red solid contours represent positive SSHA, whereas blue dashed contours represent negative SSHA or zero.

At the same time, it can be seen from Figure 3d that after LionRock passed (September 1, 2016), the position of cold and warm eddies and their radii changed significantly. After the typhoon passed, the cold eddies increased and moved toward the area close to the typhoon path, and the warm eddies weakened and moved away from the typhoon path. In particular, on August 25, the typhoon reached the turning point and a new cold eddy was generated at the turning point (box A in Figure 3b). At 2:00 a.m. on August 26, the typhoon turned from southwest to northeast, and the cold eddy generated in the box A disappeared. On August 27, the typhoon traveled to the box B region, forming a new strong cold eddy on the left side of the path (Figure 3c). LionRock also strengthened the cold eddies in the southwest and northeast to some extent.

Figure 4 shows the change in SSHA at the centers of a warm eddy (at 29.5°N, 137.625°E) and a cold eddy (at 25.375°N, 134.125°E) on the LionRock path. As the figure shows, the warm eddy was affected twice by the typhoon, and the warm eddy itself showed an increasing trend. On the day before or on the day the typhoon passed, the warm eddy center showed a slight increasing trend. After the typhoon passed, the SSHA of the warm eddy center stopped increasing, or the increase was significantly reduced. The cold eddy (located at 25.375°N, 134.125°E) was also affected by the

Preprints (www.preprints.org) | NOT PEER-REVIEWED | Posted: 15 August 2018 doi:10.20944/preprints201808.0276.v1

-reviewed version available at *Impact of Major Typhoons in 2016 on Sea Surface Features in the Northwestern Pacific* **2018**, *10*, 1326; doi:10.3390/w1010

typhoon twice. The SSHA at the center of the cold eddy slightly increased on the day of the typhoon crossing and then decreased significantly thereafter. On August 23, the SSHA of the location of the cold eddy center continued to increase before the typhoon transit, and the increase strengthened on the day of the typhoon transit. After that, the SSHA growth stopped and fell rapidly. On August 28, during the second impact of the typhoon, the SSHA of the cold eddy center also increased significantly, and then SSHA fell rapidly.

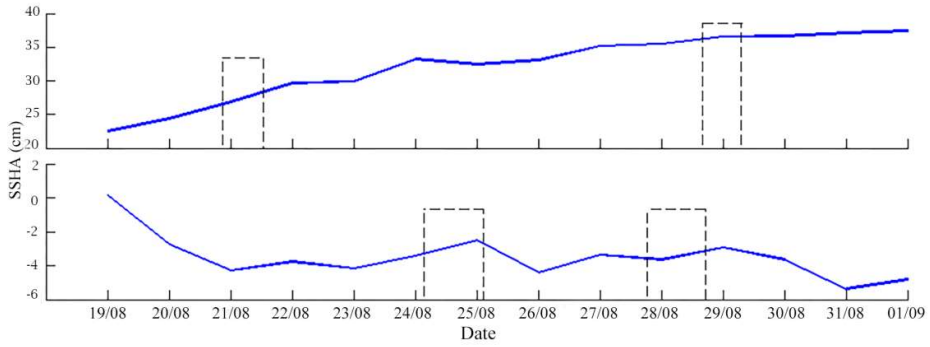

Figure 4. Variations in SSHA at the center of the warm eddy (upper) and the cold eddy (bottom) in the Typhoon LionRock passing regions. Black dashed boxes indicate where the cold or warm eddy was affected by the typhoon.

Figure 5 shows the maximum wind speed and the typhoon center pressure at various points along the typhoon path, as well as the day's SSHA. Two different degrees of typhoon enhancement (wind speed increase and pressure decrease) occurred after LionRock passed the high SSHA area and continued for some time. On August 24, the typhoon passed the high value SSHA zone (15–30 cm), the maximum wind speed of the typhoon increased from 30 to 50 m/s, and the central pressure rapidly dropped from 980 hpa to 940 hpa. From August 27 to August 29, LionRock passed through a relatively high-value SSHA area twice (>15 cm). The center wind speed increased twice, from 42 s to 52 m/s, and the center pressure decreased by 20 hpa. However, when the typhoon passed through regions with low SSHA values, it maintained its strength or was weakened to a certain extent.

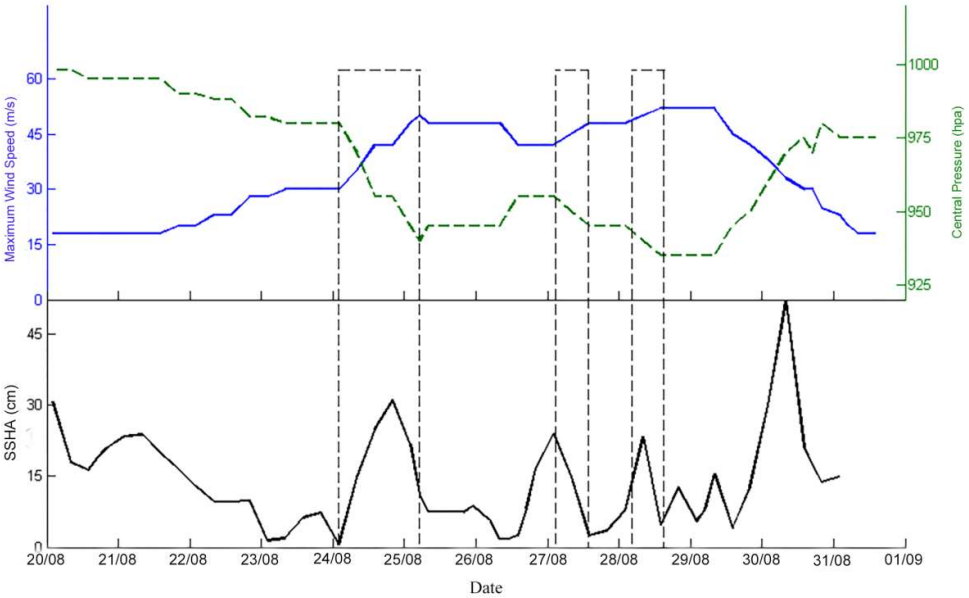

Figure 5. Variations in maximum wind speed (blue solid line) and central pressure (green dotted line) of the Typhoon LionRock (**upper**), and change in SSHA (black solid line, **bottom**) on the path of Typhoon LionRock. Black dotted boxes indicate where the typhoon changed dramatically.

Preprints (www.preprints.org) | NOT PEER-REVIEWED | Posted: 15 August 2018 doi:10.20944/preprints201808.0276.v1

-reviewed version available at *Impact of Major Typhoons in 2016 on Sea Surface Features in the Northwestern Pacific* **2018**, *10*, 1326; doi:10.3390/w1010

3.2. Meranti and Malakas

Typhoon Meranti formed on the afternoon of September 10, 2016. It strengthened into a typhoon (at 17.6°N, 131.7°E) on the early morning of September 12, strengthened into a strong typhoon at 8:00 a.m. on September 12 (at 18.0°N, 130.4°E), and strengthened to a super typhoon at 18.1°N, 129.9°E) at 11:00 a.m. on September 12. In 24 h, the wind speed of Meranti increased from 25 to 62 m/s. This meant Meranti was a rapidly increasing typhoon. At 2:00 p.m. on September 13, Meranti reached its peak intensity and the maximum wind speed near its center reached 70 m/s (over Beaufort Scale 17), stronger than the peak strength of this year's No. 1 typhoon, Nibbert (65 m/s, 17 or above). It was the strongest typhoon in the global sea area during in 2016. Meranti traveled northwest all the way to the south of Taiwan, and on September 15, it landed on the coast of Xiangan District, Xiamen, Fujian, China (at 24.57°N, 118.23°E).

As Typhoon Meranti was developing, another tropical depression was occurring near the typhoon formation at 08:00 a.m. on September 13, 2016, and it gradually developed into Typhoon No. 15, Malakas (at 15.8°N, 132.1°E). Malakas made its way to the northwest at the beginning of its generation, and it gradually developed into a strong typhoon. It turned northward on the southeastern side of Taiwan on September 17 and then turned northeast on September 18. The intensity of the system continued to be strong. After landing on the southern side of Kyushu in Japan on September 19, it gradually decreased.

Although Meranti was very intense, it did not have a strong cooling effect. It only caused a small degree of cooling in the southwestern part of the Philippines and the east side of Taiwan, with a maximum temperature drop of about 2 °C (Figure 6a). The largest area of cooling was close to the strong cold eddy shown in zone C in Figure 7a. Malakas caused a large range of cooling, and cooling was concentrated on the right side of the typhoon path (Figure 6b).

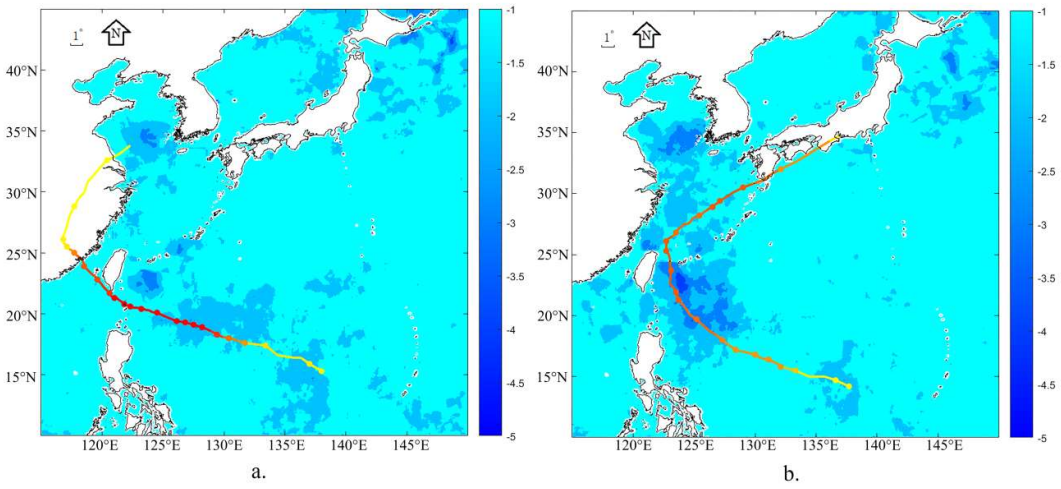

Figure 6. (**a**) Map of cooling distribution after Typhoon Meranti passed. (**b**) Map of cooling distribution after Typhoon Malakas passed. The color bar represents the degree of cooling in °C. The color of the typhoon path is consistent with Figure 1.

Preprints (www.preprints.org) | NOT PEER-REVIEWED | Posted: 15 August 2018 doi:10.20944/preprints201808.0276.v1

-reviewed version available at *Impact of Major Typhoons in 2016 on Sea Surface Features in the Northwestern Pacific* **2018**, *10*, 1326; doi:10.3390/w1010

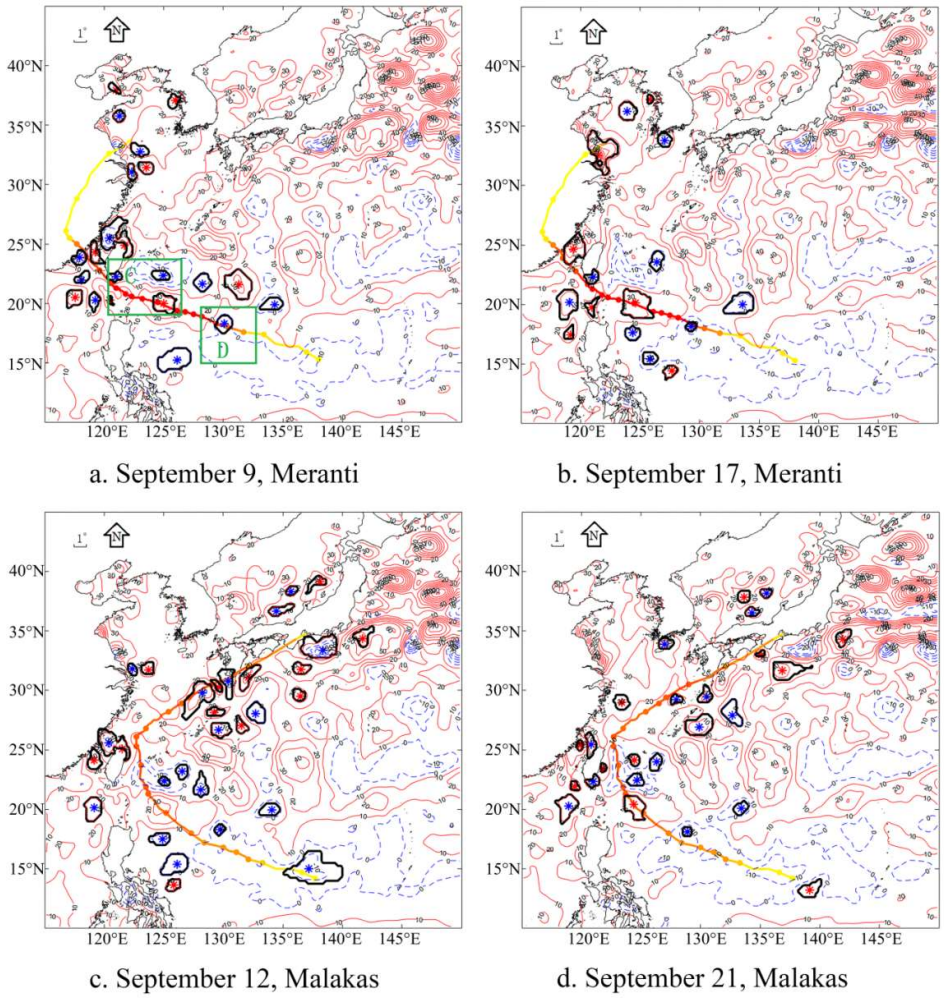

Figure 7. Map of the cold and warm vortexes distribution caused by Typhoons Meranti and Malakas. (**a**) Before Typhoon Meranti passed (September 9, 2016). (**b**) After Typhoon Meranti passed (September 17, 2016). (**c**) Before Typhoon Malakas passed (September 12, 2016). (**d**) After Typhoon Malakas passed (September 21, 2016). The color on the typhoon path is consistent with Figure 1. The bold black solid line outside the blue * (cold eddy) and the red * (warm eddy) represents the boundary of that eddy. Red solid contours represent positive SSHA, whereas blue dashed contours represent negative SSHA or zero.

The formation dates of Typhoons Meranti and Malakas were quite close to each other and their affected areas were similar. The degree of SST cooling caused by them, however, was considerably different. The main reason that the two typhoons caused a great difference in cooling may be that Meranti's path had a high SSHA level (Figure 7a). At the same time, after Typhoon Meranti crossed, the area's SSHA was reduced to some extent (Figure 7b), and the SSHA distribution also changed. This created favorable conditions for Typhoon Malakas to cool down. At the same time, Meranti moved quickly on the ocean, and the time of interaction between Meranti and its passage through the sea area was short, and this may also be the cause of its limited impact.

After the two typhoons passed the sea area, the SSHA in the sea area showed different degrees of reduction (Figure 7). In particular, after the two typhoons strengthened, the existing warm eddy (at 20°N, 124.75°E in Figure 7a, box C) disappeared. Figure 8 shows the change in SSHA between the warm eddy and the cold eddy at 17.25°N, 129.875°E (Figure 7a, box D) in the two typhoon-passing regions. It can be seen from the figure that the SSHA levels of the cold and warm eddy centers slightly increased on the day before the typhoon or the day of the typhoon, and then the SSHA of the

Preprints (www.preprints.org) | NOT PEER-REVIEWED | Posted: 15 August 2018 doi:10.20944/preprints201808.0276.v1

-reviewed version available at Impact of Major Typhoons in 2016 on Sea Surface Features in the Northwestern Pacific 2018, 10, 1326; doi:10.3390/w1010

cold and warm eddy centers decreased. Meranti's transit caused a greater reduction than Malakas in the SSHA level. The SSHA level had already fallen somewhat during the pass of Malakas, which caused a certain degree of cooling after it passed.

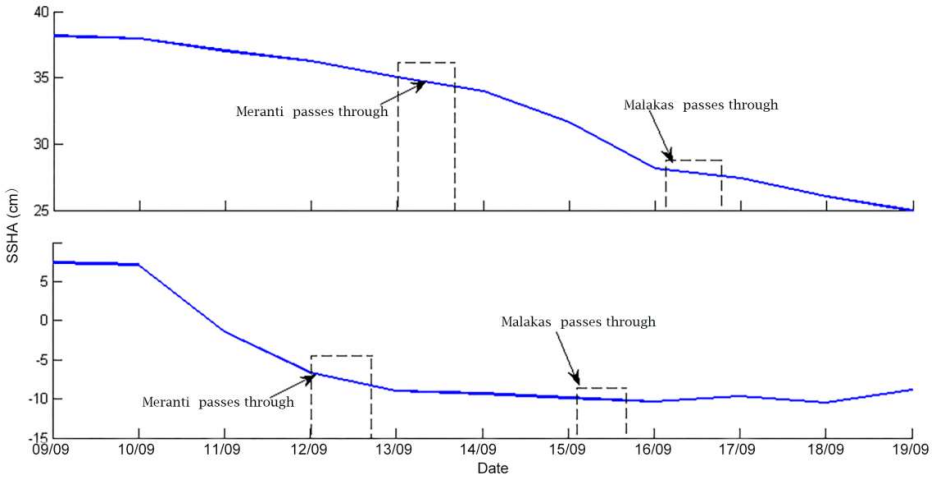

Figure 8. The change in SSHA at the center of the warm eddy (**upper**) and the cold eddy (**bottom**) in Typhoons Meranti and Malakas passing regions. The black dashed boxes indicate where the cold or warm eddy is affected by the typhoon.

As shown in Figure 9, the SSHA level of the area through which Meranti passed was relatively high (20–40 cm), which may be one of the reasons for Meranti's strength (maximum wind speed of 70 m/s), as typhoon enhancement occurs in high-value SSHA regions. At 12:00 p.m. on September 12, when the typhoon passed a SSHA area with a relatively high value of 20–40 cm, the maximum wind speed of the typhoon increased from 62 to 70 m/s, and the system grew into a super typhoon. However, when Meranti passed an area with a relatively low SSHA value, the typhoon maintained its original strength or changed only little. In addition, the apparent weakening of Meranti occurred when it arrived on land.

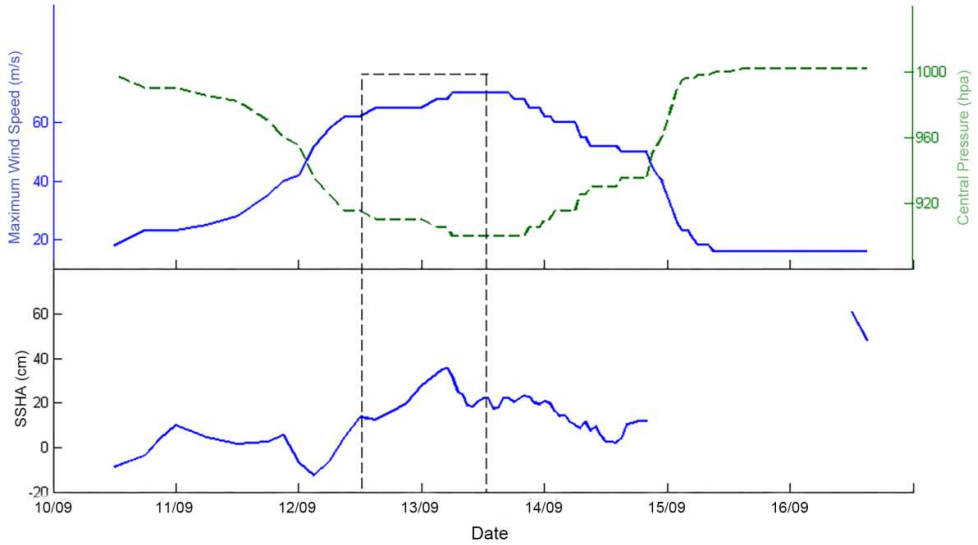

Figure 9. Variations in maximum wind speed (blue solid line) and central pressure (green dotted line) of Typhoon Meranti (**upper**), and change in SSHA (blue solid line, **bottom**) on the path of

Preprints (www.preprints.org) | NOT PEER-REVIEWED | Posted: 15 August 2018 doi:10.20944/preprints201808.0276.v1

-reviewed version available at Impact of Major Typhoons in 2016 on Sea Surface Features in the Northwestern Pacific 2018, 10, 1326; doi:10.3390/w1010

Typhoon Meranti. Black dotted boxes indicate where the typhoon changed dramatically. The part where the line suddenly disappears in the SSHA is when the typhoon passed onto land.

Malakas' history includes three distinct growths and two reductions, shown in Figure 10. The three growths occurred after Malakas passed an area with a relatively high SSHA value. Malakas continued to grow after being generated, on September 14, 2016 from 9:00 a.m. to 9:00 p.m. Malakas passed an area with a relatively low SSHA value (−12–2 cm), and the typhoon's growth stagnated. The maximum wind speed and center pressure of typhoon were maintained. From September 15 at 9:00 a.m. to 8:00 a.m. on September 16, Malakas passed through an area with a relatively high SSHA value (20–40 cm). The maximum wind speed of the typhoon increased from 42 to 50 m/s, and the central pressure dropped by 10 hpa. From September 15 at 3:00 p.m. to 9:00 p.m. on September 17, Malakas passed through an area with a relatively low SSHA value (−7–3 cm). After the typhoon maintained its strength for a period, it weakened and then passed through an area with a relatively high SSHA value. Then the typhoon strengthened again at 3:00 p.m. on September 18, 2016.

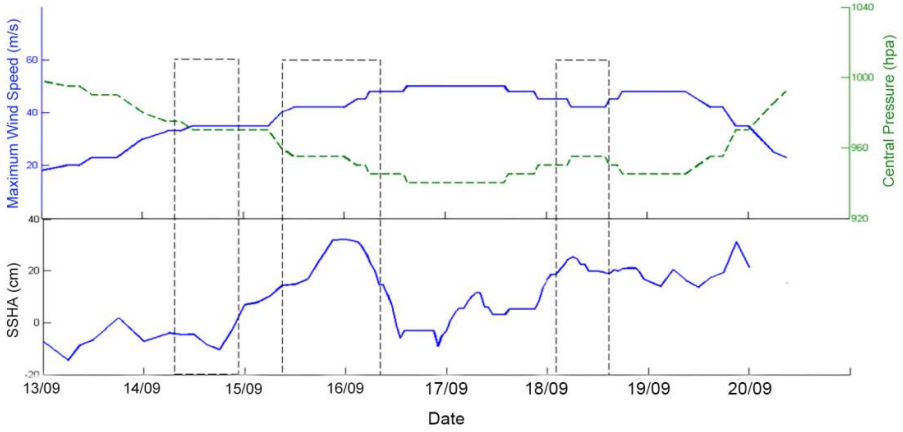

Figure 10. Similar to Figure 9 but for Typhoon Malakas.

3.3. Megi

Typhoon Megi was generated on the Northwest Pacific Ocean 2140 km south of Taitung City, Taiwan Province at 8:00 a.m. on September 23, 2016. After the typhoon was generated, it headed northwest toward Taiwan Island. On September 25, it became a strong tropical storm at 19.4°N, 139.8°E. It became a super typhoon on September 27, with a center pressure of 935 hpa and a maximum wind speed of 52 m/s. On the same day, it landed in Hualian County, Taiwan and weakened after landing. Then, it landed in Hui'an County, Fujian, China through the Taiwan Strait.

As shown in Figure 11, the cooling of the Typhoon Megi path area is obvious. The maximum cooling temperature was greater than 5 °C, and the resulting cooling distribution did not stop at the right side of the path. In the early period of typhoon development, it caused a temperature drop of 1–2 °C. The cooling area was mainly distributed on the left side of the typhoon's path. On September 24, Megi developed from a tropical depression to a tropical storm, causing a temperature drop of 1–2 °C on the right side of the typhoon path and gradually strengthening into a typhoon. On both sides of the typhoon path, we found a significant temperature drop of more than 3 °C. On September 27, Megi developed into a super typhoon and caused strong cooling (>5 °C) centered on the typhoon track area. Comparing Figures 11 and 12, the positions of cooling centers match well those of the cold eddies, and the more cold eddies there are, the more obvious the cooling. On the contrary, in areas where the warm eddies were strong, the cooling was significantly lower than in the surrounding area.

Preprints (www.preprints.org) | NOT PEER-REVIEWED | Posted: 15 August 2018 doi:10.20944/preprints201808.0276.v1

-reviewed version available at Impact of Major Typhoons in 2016 on Sea Surface Features in the Northwestern Pacific 2018, 10, 1326; doi:10.3390/w1010

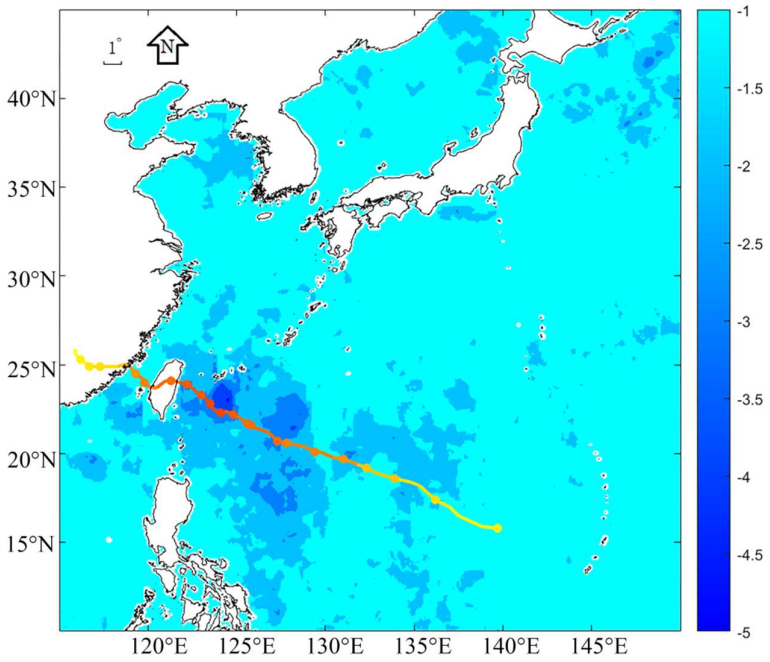

Figure 11. Map of cooling distribution after Typhoon Megi transit. The color bar value represents the degree of cooling in °C. The color of the typhoon path is consistent with Figure 1.

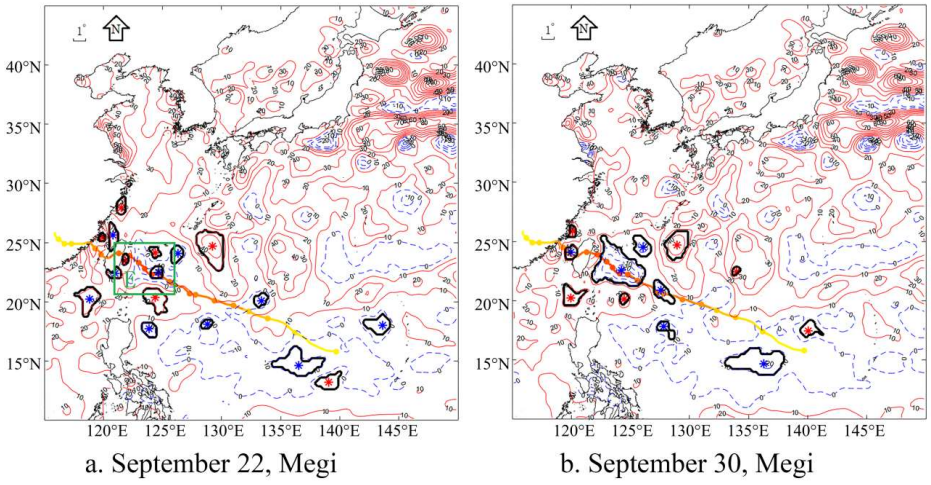

Figure 12. Map of the cold and warm eddy distribution caused by Typhoon Megi (**a**) before passage (September 22, 2016) and (**b**) after passage (September 30). The color on the typhoon path is consistent with Figure 1. The bold black solid line outside the blue * (cold eddy) and the red * (warm eddy) represents the boundary of that eddy. Red solid contours represent positive SSHA, whereas blue dashed contours represent negative SSHA or zero.

After Megi passed through the research area, the SSHA in the area demonstrated a certain degree of reduction (Figure 12). Comparing Figure 12a with 12b, there was a small cold eddy on the southeast side of Taiwan Island (Figure 12a, box E). After the typhoon passed, the smaller cold eddies merged and strengthened, and it moved toward the area close to the typhoon path. The SSHA of the cold eddy center was reduced from −15 to −30 cm and the radius of the cold eddy increased from 30 to 200 km.

As shown in Figure 13, at the beginning of Megi's formation, the area Megi passed was a high-value SSHA area (0–20 cm), and the maximum wind speed and pressure in the typhoon center

Preprints (www.preprints.org) | NOT PEER-REVIEWED | Posted: 15 August 2018 doi:10.20944/preprints201808.0276.v1

-reviewed version available at Impact of Major Typhoons in 2016 on Sea Surface Features in the Northwestern Pacific 2018, 10, 1326; doi:10.3390/w1010

continued to grow until it became a strong typhoon with a maximum center wind speed if 52 m/s and center pressure of 935 hpa. From 3:00 p.m. on September 26 to 1:00 a.m. on September 27, after the typhoon passed an area with a SSHA low value (−13–0 cm), the typhoon intensity weakened after being maintained for some time. The maximum wind speed of the typhoon center dropped to 40 m/s before the typhoon landed in Taiwan, and the central pressure increased to 960 hpa. After landing in Taiwan, Megi continued to weaken.

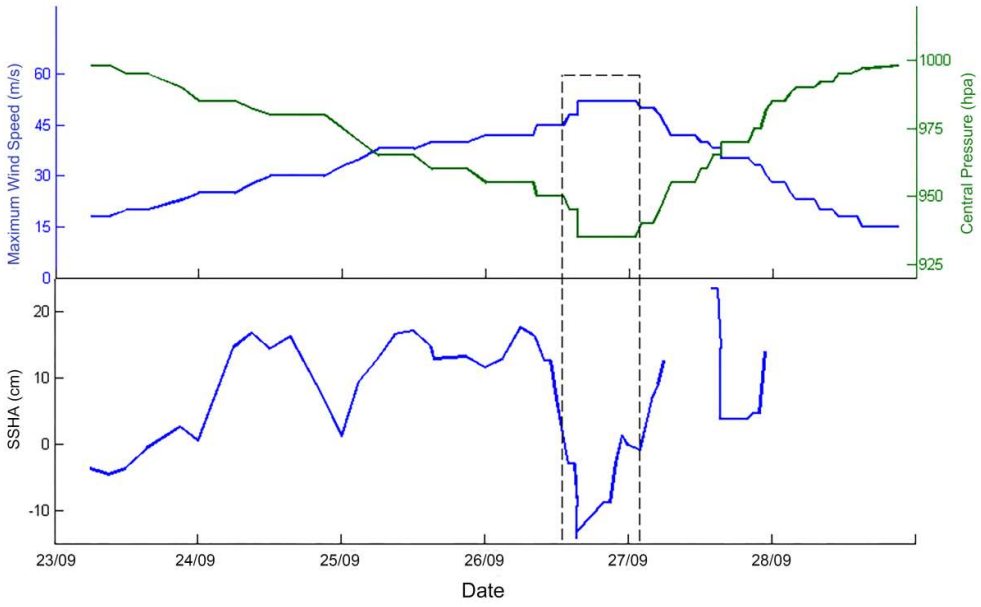

Figure 13. Variations in maximum wind speed (blue solid line) and central pressure (green dotted line) of Typhoon Megi (**upper**), and change in SSHA (blue solid line, **bottom**) on the path of Typhoon Megi. Black dotted box indicates where the typhoon changed dramatically. The part where the line suddenly disappears in the SSHA is when the typhoon passed onto land.

3.4. Chaba

Typhoon Chaba was formed in the Northwestern Pacific on September 28, 2016. Its center was located on the ocean 580 km northeast of Guam in the United States (14.6°N, 150.0°E). After being generated, it traveled westward at a speed of 20–25 km per hour to the vicinity of the Malakas generation site. Then it turned to the northwest and became a super typhoon at 8:00 a.m. on October 2. The minimum pressure in the center reached 920 hpa. The maximum wind speed reached 60 m/s. The typhoon went north to east of the East China Sea, and the strong typhoon continued until 7:00 p.m. on October 4, 2016. Then it weakened and turned to the northeast and finally wiped the coast near South Korea's Pusan. Later, it moved into the Sea of Japan and weakened into an extratropical cyclone.

Preprints (www.preprints.org) | NOT PEER-REVIEWED | Posted: 15 August 2018 doi:10.20944/preprints201808.0276.v1

-reviewed version available at Impact of Major Typhoons in 2016 on Sea Surface Features in the Northwestern Pacific 2018, 10, 1326; doi:10.3390/w1010

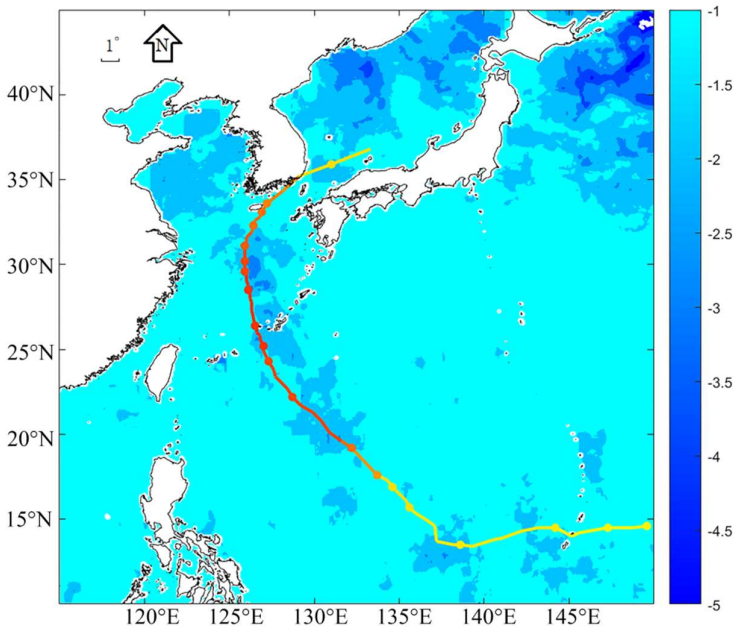

Figure 14. Map of cooling distribution after Typhoon Chaba passed. The color bar value represents the degree of cooling in °C. The color of the typhoon path is consistent with Figure 1.

When Chaba was still in the development stage, it traveled westward, causing the SST to drop by 1–2 °C (Figure 14). Most of the cooling area was located on the left side of the path, and then the typhoon turned to the northwest and gradually strengthened into a super typhoon, causing a significant reduction in the SST (>2 °C). The sea surface cooling caused by Typhoon Chaba was mainly distributed in areas with low SSHA values. Compared to those of the previous typhoons, the cooling effect caused by Chaba was relatively small. The main reason may be that the SST significantly dropped, and the seawater mixed layer deepened. The water temperature of the shallow sea water was slightly different than the SST.

Similarly, Chaba caused a certain degree of decline in the SSHA value of the area through which it passed. After the typhoon passed, the area's low SSHA value increased and a strong cold eddy was generated in the typhoon's track (Figure 15b, box F). After the typhoon transited, the warm eddy around the typhoon path gradually weakened or even disappeared. For example, before the typhoon crossed this sea area, there was a warm eddy in the eastern part of Taiwan Island (Figure 15a, box G). After the typhoon transited, the main body of the warm eddy turned away from the typhoon path, and its intensity weakened.

Preprints (www.preprints.org) | NOT PEER-REVIEWED | Posted: 15 August 2018 doi:10.20944/preprints201808.0276.v1

-reviewed version available at *Impact of Major Typhoons in 2016 on Sea Surface Features in the Northwestern Pacific* **2018**, *10*, 1326; doi:10.3390/w1010

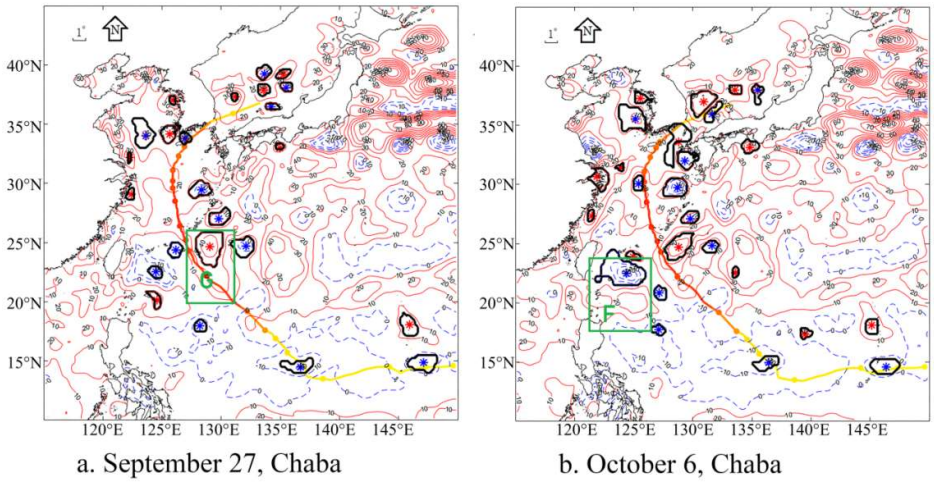

Figure 15. Map of the cold and warm eddy distribution caused by Typhoon Chaba: (**a**) before Typhoon Chaba passed (September 27, 2016) and (**b**) after Typhoon Chaba transit (October 6, 2016). The color on the typhoon path is consistent with Figure 1. The bold black solid line outside the blue * (cold eddy) and the red * (warm eddy) represents the boundary of that eddy. Red solid contours represent positive SSHA, whereas blue dashed contours represent negative SSHA or zero.

As shown in Figure 16, at the beginning of the generation of Chaba, the SSHA value of the sea area where the typhoon passed was small (−17 to 6 cm), and the maximum wind speed and pressure of the typhoon center did not change much. From September 30 to October 2, 2016, the typhoon passed through a region with a high SSHA value (8–22 cm) and continued to strengthen and maintain its strength for a long time. When the typhoon was strongest, the wind speed reached 60 m/s and the center pressure was 920 hpa. After passing through the shallow sea area, the typhoon gradually weakened and disappeared.

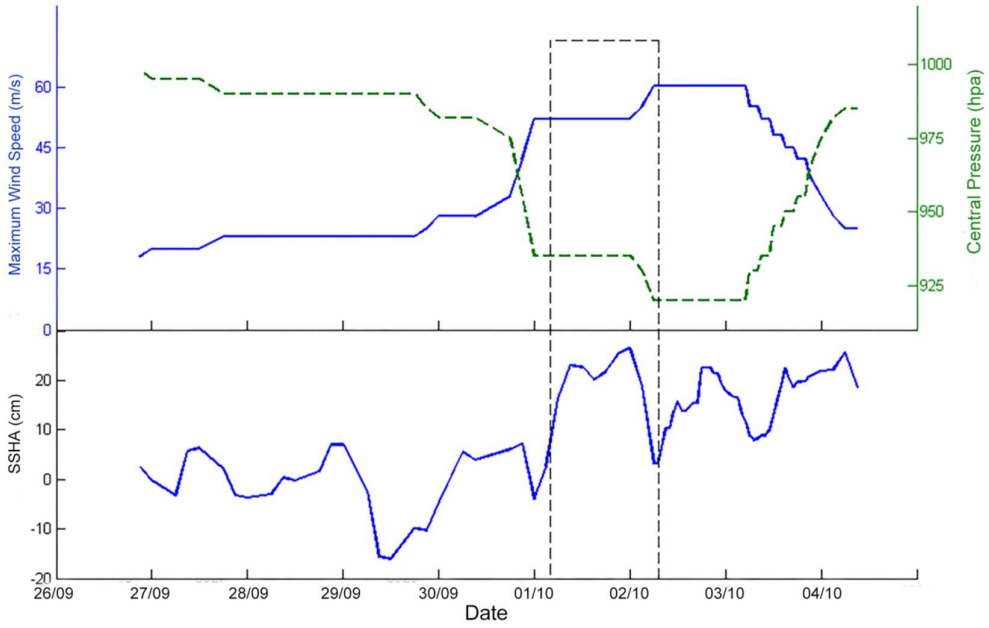

Figure 16. Variations in maximum wind speed (blue solid line) and central pressure (green dotted line) of Typhoon Chaba (**upper**), and change in SSHA (blue solid line, **bottom**) on the path of Typhoon Chaba. Black dotted box indicates where the typhoon changed dramatically.

Preprints (www.preprints.org) | NOT PEER-REVIEWED | Posted: 15 August 2018 doi:10.20944/preprints201808.0276.v1

-reviewed version available at Impact of Major Typhoons in 2016 on Sea Surface Features in the Northwestern Pacific 2018, 10, 1326; doi:10.3390/w1010

4. Discussion

4.1. Impact of Tropical Cyclones on SST

To our knowledge, there have been many observations and simulations of sea temperature changes caused by typhoons, but most have been limited to the study of some cases. We studied five consecutive typhoons that occurred in the Western Pacific in 2016, including LionRock (1610), Meranti (1614), Malakas (1616), Megi (1617), and Chaba (1618). Through the analysis of SST data and SSHA data from ocean remote sensing, we found that the typhoon-induced cooling of the sea surface is roughly distributed on the left and right sides of the typhoon track, with a range of about 100 km. The cooling area is approximately circular. This is consistent with the results reported by Yang and Tang [27], who conducted statistical analysis of typhoons across the South China Sea over many years. However, we have come to a more detailed conclusion by analyzing the distribution of cooling caused by various typhoons and the distribution of SSHA before the typhoon passes over a sea area. We found that the area where the SSHA was greater than zero before the typhoon crossed, and the cooling rate after the typhoon passed was less than 3 °C. In areas where the SSHA was less than zero before the typhoon crossed, the cooling range after the typhoon passes was usually greater than 3 °C. The cooling center was closer to the center of the cold eddies. Among them, Typhoon LionRockLionRock caused the largest cooling area, as shown in Figure 2. In the warm eddies area where the SSHA was positive, the degree of cooling was small, and was concentrated in the range of 2 to 3 °C. However, in the cold eddies area near the typhoon path with negative SSHA, the cooling rate was relatively large, both above 3 °C and even reaching 5 °C. Moreover, at the turning point of Typhoon LionRockLionRock, a new cold eddy was formed, and the cooling rate was significantly higher than other regions (>5 °C), which is consistent with the research findings of Jiang et al. [18]. Typhoon Megi had an obvious cooling in the path area, as shown in Figure 9. The degree of cooling caused by the early typhoon was relatively small. However, after Megi developed into a super typhoon, it caused significant cooling in the path area. In addition, the location of the cooling area caused by Megi was basically the same as the distribution of cold eddies, and the cooling was more obvious in the area where the cold eddies were strong, while in the warm eddy areas, the cooling was lower than the surrounding area.

4.2. Relationship Between Tropical Cyclones and SSHA Distribution

We found that when a typhoon crosses over a sea area, it causes SSHA to respond strongly. The main action was that the SSHA obviously decreased. After Typhoon LionRockLionRock passed over the sea, the cold eddies strengthened, while the warm eddies weakened, and the center of the cold eddy moved toward the area close to the typhoon path, while the warm eddy moved away from the typhoon path. After the passage of Typhoons Meranti and Malakas, SSHA showed a different degree of reduction. After Typhoon Megi passed over, the small cold eddy that existed before the typhoon merged and intensified, and moved closer to the typhoon path. Similarly, the passage of Typhoon Chaba also created a low value SSHA area, which was located in the southwest of the northwestern Pacific greater, and generated a stronger cold eddy at the typhoon path, which is consistent with the research conclusions of Yang et al. [21].

We also found that the mesoscale eddies, which existed in the upper ocean before the typhoon, not only played an important role in the extent and location of the cooling of the sea surface, but also had an important impact on the typhoon intensity during the typhoon passage. During Typhoon LionRockLionRock, two different degrees of typhoon intensification occurred after the typhoon passed the higher (or warm eddies) areas of SSHA. However, when the typhoon passed through regions with low SSHA values, it maintained a constant intensity or weakened to a certain extent. The apparent weakening of Typhoon Meranti also occurred when it passed SSHA-reduced areas or arrived on land, and the three growths in the life of Malakas occurred after passing through the relatively high value area of SSHA. At the beginning of Typhoon Megi, when it passed through the area with high SSHA, the wind speed increased, the pressure decreased, and the typhoon continued to grow. However, at the beginning of Typhoon Chaba, the SSHA of the passing sea area was small,

Preprints (www.preprints.org) | NOT PEER-REVIEWED | Posted: 15 August 2018 doi:10.20944/preprints201808.0276.v1

-reviewed version available at Impact of Major Typhoons in 2016 on Sea Surface Features in the Northwestern Pacific 2018, 10, 1326; doi:10.3390/w1010

so the maximum wind speed and center pressure of the typhoon did not change much. The above results support the view that a typhoon passing through a warm eddy region (i.e., relatively high SSHA area) will increase in intensity. After passing through a cold eddy region (i.e., relatively low SSHA area), the typhoon intensity will remain unchanged or gradually weaken.

5. Conclusions

In the present work, five strong or super typhoons in the Northwestern Pacific Ocean that occurred in 2016 were selected and satellite altimeter data and SST data were used to analyze typhoon-induced changes in the marine environment.

After a typhoon passed, it caused a significant cooling of the sea surface. The degree of reduction in SST was determined by the intensity, the travelling speed of the typhoon, and the pre-existing sea surface conditions. In general, the SST obviously decreased after a typhoon passed when the initial SSHA was negative, and the cooling centers were consistent with the centers of the cold eddies. On the other hand, if the initial SSHA was positive, the degree of SSC was relatively unobvious.

After the typhoon passed, it had certain influence on the SSHA. One day before or on the day the typhoon crossed an area, the SSHA increased slightly, which was mainly caused by the low sea level pressure. Due to the wind-induced Ekman pumping and the decrease in SST, after the typhoon passed through, the SSHA obviously decreased. Typhoons also have a significant impact on the distribution of cold and warm eddies. Cold eddies are enhanced and their centers move toward the typhoon track. When the typhoon suddenly changes its direction, new cold eddies are generated. On the contrary, the typhoon causes warm eddies to weaken or even disappear and move away from the typhoon track.

The presence of warm eddies had a catalytic effect on the strengthening of typhoons. After a typhoon passed a relatively high SSHA (or warm eddy) region, the maximum wind speed significantly increased and the central air pressure decreased. After a typhoon passed through a relatively low SSHA (or cold eddy) region, the maximum wind speed remained unchanged or decreased.

In this article, we used SST and SSHA data to demonstrate the evolution of the marine environment during typhoons. However, we note that owing to the limits of data used, some important effects have been omitted, such as the impact of typhoon-induced ocean circulation on mesoscale eddies, the combined effect of two or more typhoons, relationship between typhoon speed and SSC, etc. Every year, a large number of typhoons pass over mesoscale eddies in the Western North Pacific. Therefore, it is important to understand typhoon-eddy interactions to improve our prediction of typhoon intensity in this region. We plan to further apply the ocean–atmosphere coupling model and use new time-series data to systematically study more typhoon events in the Western North Pacific and to address the influence of mesoscale eddies on the typhoon intensity.

Funding: This research was funded by the Ministry of Science and Technology of the People's Republic of China under grant number 2016YFC1401404, the Zhejiang Provincial Natural Science Foundation of China under grant number LY17D060003, and the Key Laboratory of Ocean Circulation and Waves of the Chinese Academy of Sciences under grant number KLOCW1704.

Acknowledgments: We would like to thank Shuangyan He, Jiawang Chen and some other colleagues from the Zhejiang University for their remarkable advice on the present work. We also deeply thank Jianlei Fan for proofreading.

Conflicts of Interest: The authors declare no conflict of interest. The founding sponsors had no role in the design of the study; in the collection, analyses, or interpretation of data; in the writing of the manuscript, and in the decision to publish the results.

Preprints (www.preprints.org) | NOT PEER-REVIEWED | Posted: 15 August 2018 doi:10.20944/preprints201808.0276.v1

-reviewed version available at Impact of Major Typhoons in 2016 on Sea Surface Features in the Northwestern Pacific 2018, 10, 1326; doi:10.3390/w1010

References

1. Chen, D.K.; Lei, X.T.; Wang, W.; Wang, G.H. Upper Ocean Response and Feedback Mechanisms to Typhoon. *Adv. Earth Sci.* **2013**, *28*, 1077–1086. (In Chinese)
2. Wada, A.; Uehara, T.; Ishizaki, S. Typhoon-induced sea surface cooling during the 2011 and 2012 typhoon seasons: Observational evidence and numerical investigations of the sea surface cooling effect using typhoon simulations. *Prog. Earth Planet. Sci.* **2014**, *1*, 11, doi:10.1186/2197-4284-1-11.
3. Heo, K.Y.; Ha, T.; Park, K.S. The effects of a typhoon-induced oceanic cold wake on typhoon intensity and typhoon-induced ocean waves. *J. Hydro-Environ. Res.* **2016**, *14*, 61–75, doi:10.1016/j.jher.2016.06.002.
4. Kuo, Y.C.; Lee, M.A.; Chern, C.S. Typhoon-induced ocean responses off the southwest coast of Taiwan. *Ocean Dyn.* **2014**, *64*, 1569–1581, doi:10.1007/s10236-014-0776-8.
5. Balaguru, K.; Taraphdar, S.; Leung, L.R.; Foltz, G.R.; Knaff, J.A. Cyclone-cyclone interactions through the ocean pathway. *Geophys. Res. Lett.* **2014**, *41*, 6855–6862, doi:10.1002/2014GL061489.
6. Price, J.F. Upper ocean response to a hurricane. *J. Phys. Oceanogr.* **1981**, *11*, 153–175, doi:10.1575/1912/10271.
7. Sanford, T.B.; Price, J.F.; Girton, J.B. Upper-Ocean Response to Hurricane Frances (2004) Observed by Profiling EM-APEX Floats. *J. Phys. Oceanogr.* **2011**, *41*, 1041–1056, doi:10.1175/2010jpo4313.1.
8. Shang, S.L.; Li, L.; Sun, F.Q.; Wu, J.Y.; Hu, C.M.; Chen, D.W.; Ning, X.R.; Qiu, Y.; Zhang, C.Y.; Shang, S.P. Changes of temperature and bio-optical properties in the South China Sea in response to Typhoon Lingling, 2001. *Geophys. Res. Lett.* **2008**, *35*, L10602, doi:10.1029/2008gl033502.
9. Yang, Y.J.; Fu, Y.F.; Sun, L.; Liu, P.; Feng, S. Responses of the upper ocean to Typhoon Tingting observed from multiplatform satellites and Argo float. *J. Univ. Sci. Technol. China* **2010**, *40*, 1–7. (In Chinese)
10. Wu, R.; Cao, X.; Chen, W. Surface wind speed-SST relationship during the passage of typhoons over the South China Sea. *IEEE Geosci. Remote Sens. Lett.* **2012**, *9*, 933–937, doi:10.1109/lgrs.2012.2185819.
11. Mahapatra, D.K.; Rao, A.D.; Babu, S.V.; Srinivas, C. Influence of coast line on upper ocean's response to the tropical cyclone. *Geophys. Res. Lett.* **2007**, *34*, 17601–17603, doi:10.1029/2007gl030410.
12. Kuo, Y.C.; Chern, C.S.; Wang, J.; Tsai, Y.L. Numerical study of upper ocean response to a typhoon moving zonally across the Luzon strait. *Ocean Dyn.* **2011**, *61*, 1783–1795, doi:10.1007/s10236-011-0459-7.
13. Subrahmanyam, M.V. Impact of typhoon on the north–west pacific sea surface temperature: A case study of typhoon kaemi (2006). *Nat. Hazards* **2015**, *78*, 569–582, doi:10.1007/s11069-015-1733-7.
14. Liu, Z.; Xu, J.; Zhu, B.; Sun, C.; Zhang, L. The upper ocean response to tropical cyclones in the northwestern pacific analyzed with Argo data. *Chin. J. Oceanol. Limnol.* **2007**, *25*, 123–131, doi:10.1007/s00343-007-0123-8.
15. Yue, X.; Zhang, B.; Liu, G.; Li, X.; Zhang, H.; He, Y. Upper ocean response to typhoon Kalmaegi and Sarika in the south china sea from multiple-satellite observations and numerical simulations. *Remote Sens.* **2018**, *10*, 348, doi:10.3390/rs10020348.
16. Lin, S.; Zhang, W.-Z.; Shang, S.-P.; Hong, H.-S. Ocean response to typhoons in the western north pacific: Composite results from Argo data. *Deep Sea Res. Part I* **2017**, *123*, 62–74, doi:10.1016/j.dsr.2017.03.007.
17. Wu, R.; Li, C. Upper ocean response to the passage of two sequential typhoons. *Deep Sea Res. Part I* **2018**, *132*, 68–79, doi:10.1016/j.dsr.2017.12.006.
18. Jiang, X.P.; Zhong, Z.; Shao, S.N.; Jiang, H.F. The variation features of SST induced by tropical cyclones over SCS. *J. Meteorol. Sci.* **2008**, *28*, 614–618. (In Chinese)
19. Liu, G.P.; Hu, J.H. Response of the mesoscale eddies to tropical cyclones in the South China Sea: A case study. *J. Oceanogr. Taiwan Strait* **2009**, *28*, 308–315. (In Chinese)
20. Yablonsky, R.M.; Ginis, I. Impact of a warm ocean eddy's circulation on hurricane-induced sea surface cooling with implications for hurricane intensity. *Mon. Weather Rev.* **2009**, *141*, 997–1021, doi:10.1175/mwr-d-12-00248.1.
21. Yang, Y.J.; Tao, X.; Sun, L.; Fu, Y.F.; Xun, S.P. Impacts of sequential typhoons on sea surface temperature and sea surface height in September 2008. *Acta Oceanol. Sin.* **2012**, *34*, 71–78. (In Chinese)
22. Lin, I.I.; Wu, C.C.; Emanuel, K.A.; Lee, I.H.; Wu, C.R.; Pun, L.F. The Interaction of Super typhoon Maemi (2003) with a Warm Ocean Eddy. *Mon. Weather Rev.* **2005**, *133*, 2635–2649, doi:10.1175/mwr3005.1.
23. Sun, L.; Yang, Y.J.; Tao, X.; Lu, Z.M.; Fu, Y.F. Strong enhancement of chlorophyll a concentration by a weak typhoon. *Mar. Ecol. Prog. Ser.* **2010**, *404*, 39–50, doi:10.3354/meps08477.
24. Zhang, W.Z.; Lin, S.; Jiang, X.M. Influence of Tropical Cyclones in the Western North Pacific. In *Recent Developments in Tropical Cyclone Dynamics, Prediction, and Detection*; Anthony, R.L., Ed.; IntechOpen: London, UK, 2016; pp. 3–24, ISBN 95351270399535127020.

Preprints (www.preprints.org) | NOT PEER-REVIEWED | Posted: 15 August 2018 doi:10.20944/preprints201808.0276.v1

-reviewed version available at Impact of Major Typhoons in 2016 on Sea Surface Features in the Northwestern Pacific 2018, 10, 1326; doi:10.3390/w1010

25. Lin, J.R.; Tang, D.L.; Lou, Q.S. The impact of Super Typhoon Nanmadol on the chlorophyll a, temperature, salinity and dissolved oxygen in the northern South China Sea. *Ecol. Sci.* **2015**, *34*, 9–14. (In Chinese)
26. Ma, Z.; Fei, J.; Liu, L.; Huang, X.; Cheng, X. Effects of the cold core eddy on tropical cyclone intensity and structure under idealized air–sea interaction conditions. *Mon. Weather Rev.* **2013**, *141*, 1285–1303, doi:10.1175/mwr-d-12-00123.1.
27. Yang, X.; Tang, D. Location of sea surface temperature cooling induced by typhoon in the South China Sea. *J. Trop. Oceanogr.* **2010**, *29*, 26–31. (In Chinese).
28. Hu, J.; Hiroshi, K. Detection of cyclonic eddy generated by looping tropical cyclone in the northern South China Sea: A case study. *Acta Oceanol. Sin.* **2004**, *23*, 213–224.
29. Morey, S.L.; Bourassa, M.A. Modeling studies of the upper ocean response to a tropical cyclone. *Ocean Dyn.* **2006**, *56*, 594–606, doi10.1007/s10236-006-0085-y
30. Liu, J.; Dai, J.; Xu, D.; Wang, J.; Yuan, Y. Seasonal and interannual variability in coastal circulations in the northern south China sea. *Water* **2018**, *10*, 520, doi:10.3390/w10040520.
31. Wu, C.C.; Huang, T.S. A New Look at the Binary Interaction: Potential Vorticity Diagnosis of the Unusual Southward Movement of Tropical Storm Bopha (2000) and Its Interaction with Super Typhoon Saomai (2000). *Mon. Weather Rev.* **2003**, *131*, 1289–1300.